AIAA JOURNAL
Vol. 34, No. 5, May 1996

Interaction of Missile Nose-Tip Vortices with a Control Surface

John W. Kiedaisch* and Mukund Acharya†
Illinois Institute of Technology, Chicago, Illinois 60616

The interaction between vortices forming at the nose tip of a missile model and a single fin located down the axis of the model was investigated experimentally for a range of axial fin positions [$2.6 < (x/d)_f < 9.4$], azimuthal fin positions (-180 deg $< \phi < -180$ deg), and Reynolds number ($6 \times 10^3 < Re_d < 3.4 \times 10^4$) for two angles of attack, 30 and 45 deg. Symmetric, attached vortices formed over the model at the lower angle of attack, whereas the vortices were asymmetric when the angle of attack was increased to 45 deg. The interaction was documented using flow visualization and mean pressure measurements on the fin surfaces. The pressure data were used to compute the normal force coefficients on the fin. The effects of the interaction on the fin are described; in particular, the similarities and differences in the flowfield at the two angles of attack are discussed for one axial fin location [$(x/d)_f = 7.1$].

Nomenclature

C_{fp}	= normal force coefficient, port surface of fin
C_{fs}	= normal force coefficient, starboard surface of fin
C_{ft}	= total normal force coefficient
C_p	= pressure coefficient
d	= model diameter
Re_d	= Reynolds number based on model diameter
x	= axial distance along model from nose tip
x'	= axial distance from leading edge of fin
$(x/d)_f$	= dimensionless distance from nose to leading edge of fin
y'	= transverse (spanwise) distance from root chord of fin
α	= pitch angle
ϕ	= azimuthal angle of fin, measured from leeward ray

Introduction and Background

SEPARATED, vortical flows are found around slender bodies of revolution at angles of attack (AOAs), such as missile and rocket geometries, and in the forebody region of aircraft. Other examples include the flow over delta-shaped aircraft or helicopters and the dynamic-stall vortex that forms over the suction surface of a pitching wing. In several missile, rocket, helicopter, and aircraft applications, the interaction of vortical structures with surfaces and appendages plays a very important role in determining the agility and overall performance of the craft. Such vortex–surface interaction therefore continues to be the subject of investigation by both experiments and computational modeling. For example, Mendenhall and Perkins[1] developed a calculation procedure for the prediction of nonlinear aerodynamic characteristics of missiles at high AOAs in subsonic flow. Their results included predictions of the vortex-induced effects on the normal force coefficients for a single fin mounted approximately 10 diameters from the missile nose. Washburn et al.[2] conducted experiments to examine the interaction between vortices forming over a sharp-edged delta wing and twin tails mounted at the rear. Their work focused on the effects of tail position on the vortex trajectories and vortex breakdown, as well as fin loading and buffet. Bodstein et al.[3] developed an analytical model for the interaction of a streamwise vortex with a long plate. Their results included spanwise variations of the vortex-induced pressures on the plate and vortex trajectories over the plate.

A central feature of the flow about slender bodies at AOAs is three-dimensional flow separation, resulting in the formation of well-defined, vortical structures on the leeward side of the body. The general nature of these flows is known,[4] but the underlying mechanisms are not completely understood. Flow development depends on several parameters, including AOA, Reynolds number, Mach number, nose-tip shape, and surface conditions. The leeside flowfield is dominated by a pair of vortices that form very close to the tip of the nose and travel downstream along the missile body, eventually lifting away from the body. At lower AOAs, these vortices are symmetric, but as the angle of attack is increased, the leeside flowfield becomes increasingly complex—the vortices become asymmetric and have differing strengths and locations with respect to the missile body. This vortex system may impinge on, or interact with, fins or other control surfaces located further down the missile axis. The interaction is very complex in nature; it can modify the pressure field and, consequently, the loading on these surfaces, thereby altering the effectiveness of the surface. Vortex-induced loads are difficult to predict and cause changes in yaw, roll, and pitch motions that can be coupled in a nonlinear manner. An investigation to understand the nature and outcome of such interactions is therefore of great value.

Objectives

The overall objective of this work was to examine interactions between the nose-tip vortices and surfaces for a typical missile geometry and to understand the influence of these vortices on control surfaces such as fins and canards that may be placed at different locations along a missile body. The specific goals of the present experiments were 1) to document the interaction of the nose-tip vortices and a single, generic, control surface through flow visualization and mean pressure measurements, 2) to identify and understand the physical mechanisms that play an important role in this interaction, 3) to determine the forces on the fin that result from interaction with the vortices, and 4) to examine the effects of fin placement on the development of the vortex system.

Experiments were carried out for two AOAs chosen to obtain symmetric and asymmetric states of the nose-tip vortices. The main features of this interaction for both states are described in this paper. In particular, similarities and differences in the flowfield at the two AOAs, and the consequent effects on the interactions with the fin, are discussed for cases with the fin placed at an axial location of $(x/d)_f = 7.1$.‡

Experimental Arrangement

Wind Tunnel, Model Design, and Instrumentation

The experiments were conducted in the Andrew Fejer Unsteady Wind Tunnel at IIT's Fluid Dynamics Research Center. This is a closed-circuit, low-speed facility with a freestream turbulence level of 0.03% in the test section at its maximum velocity. The test section

Received Aug. 5, 1994; revision received Jan. 12, 1996; accepted for publication Feb. 2, 1996.

*Graduate Research Assistant, Fluid Dynamics Research Center. Student Member AIAA.
†Professor, Fluid Dynamics Research Center. Senior Member AIAA.

‡A detailed analysis of the fin interaction with both the symmetric and asymmetric vortex systems, with explanations for the azimuthal range of fin positions over which interaction occurred, and the effects of changing axial fin location is included in *AIAA Journal on Disc*, Vol. I, No. 2.

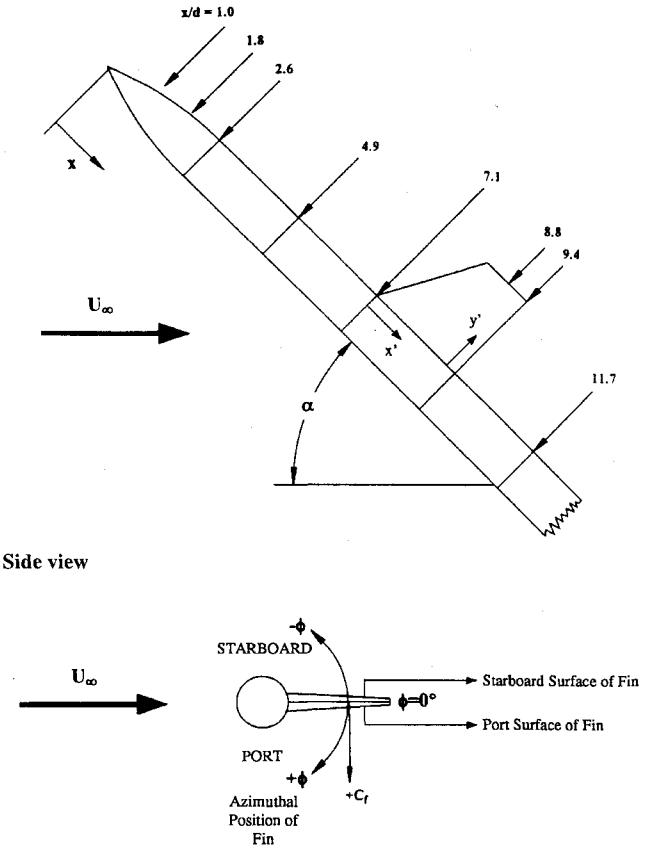

Fig. 1 Model schematic and coordinate system.

is 0.61 m square in cross section and 3.1 m in length. A positioning system allowed the model to be placed in the central region of the test section, at the desired yaw and pitch angles, through the use of three stepper motors. The ability to roll the model was built directly into its design using another small, internally mounted stepper motor. The four motors were controlled by a Masscomp minicomputer equipped with a digital-to-analog converter board and an analog-to-digital converter board. The model position was monitored by four Hewlett Packard optical encoders and codewheels, one mounted to each motor. The control code used is described in detail by Acharya et al.[5]

The model used in the present experiments had a body diameter d of 1.44 in. (3.65 cm) and a length of 20 in. (50.8 cm), including a tangent-ogive nose 3.75 in. (9.53 cm) long. A modular construction, shown schematically in Fig. 1, was used.[§] The generic fin used in the vortex–surface interaction experiments could be placed in any one of four axial locations along the body of the model (Fig. 1), by interchanging body sections. These locations are referred to as stations 1–4 in subsequent discussions. The fin had a tapered, clipped-delta shape with a chord length of 3.25 in. (8.26 cm) and a span of 3.0 in. (6.72 cm), or approximately two diameters. The sweep angle of the leading edge was 28.4 deg. The fin was 0.19 in. (0.48 cm) thick at the tip and 0.5 in. (1.27 cm) thick at the root. Two identical fins were used in the experiments: one for flow visualization and the second for pressure measurements. Both surfaces of the latter, designated the port and starboard surfaces for purposes of identification, were instrumented with pressure ports. One row of pressure ports was also located axially on the model body, along the root of the fin.[¶] The relatively large fin thickness was necessary to accommodate the pressure ports and tubing within the fin. Although in reality missile fins are thinner relative to the body radius, it was felt that the geometry used would nevertheless provide an accurate representation of many of the important features of the vortex–fin interaction. A more detailed description of the wind tunnel, model positioning system, and model design is given by Kiedaisch.[6] A laser-sheet/smoke-wire technique was used for flow visualization, and a Setra model 239 transducer was used for pressure measurements.[**]

[§]This feature is discussed in Section I of the Addenda.

[¶]A diagram of the fin and coordinates of the pressure ports are found in Fig. 1 of the Addenda.

Experimental Procedure and Parameter Ranges

Experiments were performed for two pitch angles α, 30 and 45 deg. This selection was based upon earlier work described by Acharya et al.[5] that was performed using the same facilities and model. The nose-tip vortices were symmetric at 30 deg and asymmetric at 45 deg. Care was taken to ensure that flowfield conditions remained the same throughout the experiments.

The first phase involved a detailed flow-visualization study of the vortex system and its interaction with the control surface (fin) using the laser-sheet/smoke-wire technique. All flow visualization was performed at a Reynolds number of 6×10^3 because of limitations of the smoke-wire technique at higher flow speeds. Experiments were conducted for four axial locations of the fin (see Fig. 1), identified by the axial position of the fin's leading edge $[(x/d)_f]$. At station 1, $(x/d)_f = 2.6$. At stations 2, 3, and 4, $(x/d)_f = 4.9$, 7.1, and 9.4, respectively. For each axial location of the fin, flow visualization was performed at a section through the middle of the fin for a series of azimuthal fin positions ϕ 5.4 deg apart, over the range -92 to $+92$ deg. Development of the vortices ahead of the fin was documented at several axial locations (the number varied with the axial location of the fin) for three azimuthal fin positions: 0 and ± 54 deg. At the leading and trailing edges of the fin, flow development was documented for five azimuthal fin positions: 0, ± 22, and ± 54 deg.

Pressure data were obtained on both surfaces of the fin at Reynolds numbers of 6×10^3, 2×10^4, and 3.4×10^4 for the four axial locations of the fin. Data sets were acquired at azimuthal fin positions every 5.4 deg from -178 to $+178$ deg, along with one set at 180 deg. The pressure data were nondimensionalized by the approach-flow dynamic pressure to obtain coefficient of pressure. The pressure data were also used to compute the normal-force coefficients for each side of the fin. The forces were nondimensionalized by the dynamic pressure and the fin planform area. The experimental uncertainty in the measured coefficient of pressure C_p data was estimated to be $\pm 2.1\%$ using standard small-sample methods.

Results and Discussion

Flowfield Development

At $\alpha = 30$ deg, a pair of steady, symmetric vortices dominated the wake on the leeward side of the model. Figure 2a shows the development of the vortex system at seven axial locations along the model. Each view is a cross-sectional plane perpendicular to the model axis, looking down along the axis from the nose tip. Flow is from left to right, and the fin is at $\phi = 0$ deg, corresponding to the leeward ray of the model. The starboard side is toward the top of each view, and the port side is toward the bottom.[††]

In Fig. 2a, the fin is at axial station 3 $[(x/d)_f = 7.1]$. The pair of vortices has started to form at $x/d = 1.0$. By $x/d = 1.8$, the vortices have formed and are clearly symmetric. They remain symmetric, coherent, and close to the body through $x/d = 7.1$, the leading edge of the fin. At this location, the vortices become slightly less coherent, presumably an influence of the fin. At $x/d = 8.8$, the middle of the fin, the vortices remain symmetric, but are clearly less coherent, and start to lift away from the body. The centers of the vortices are further from the leeward ray at this location because of the presence of the fin. At the trailing edge of the fin, $x/d = 9.4$, the vortices are further away from the body but otherwise unchanged. In the region of the fin, the vortices are large, symmetric, and their trajectories run close to the body. Therefore, there is a substantial interaction between the vortex system and the fin at this axial location.

The flowfield develops similarly with the fin placed at the other three axial locations. The vortex development from $x/d = 1.0$ through 7.1 with the fin at station 4$[(x/d)_f = 9.4]$ is very similar to that shown in Fig. 2a. Flow visualization for this case is described by Kiedaisch.[6] The vortices continue to grow symmetrically and remain attached to the body up to the leading edge of the fin $(x/d = 9.4)$.

[**]The instrumentation is described in more detail in Section II of the Addenda.

[††]More detail about the visualizations is provided in Section III of the Addenda.

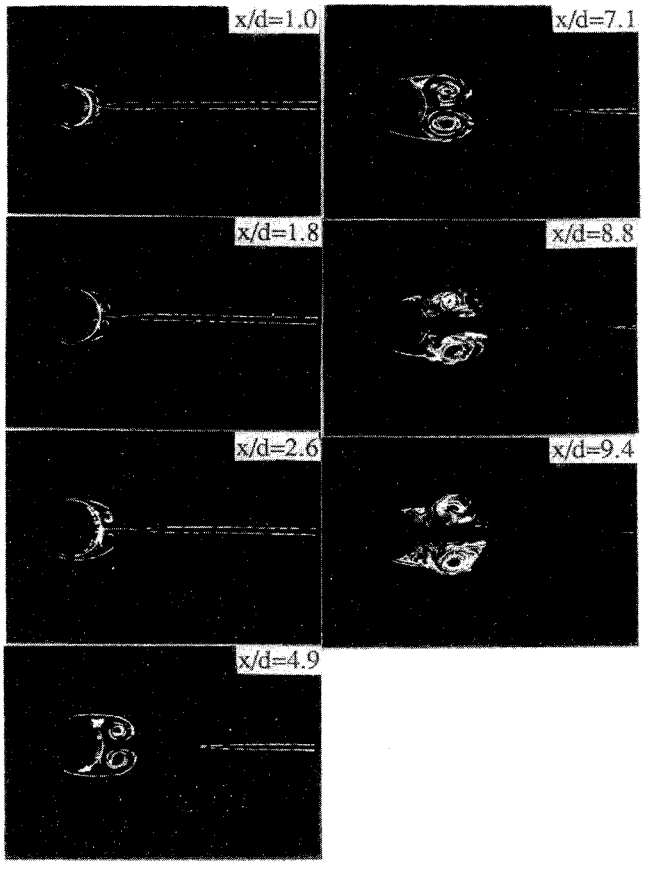

Fig. 2a Cross-sectional flow visualization showing flowfield development (α = 30 deg, ϕ = 0 deg, and $Re_d = 6 \times 10^3$).

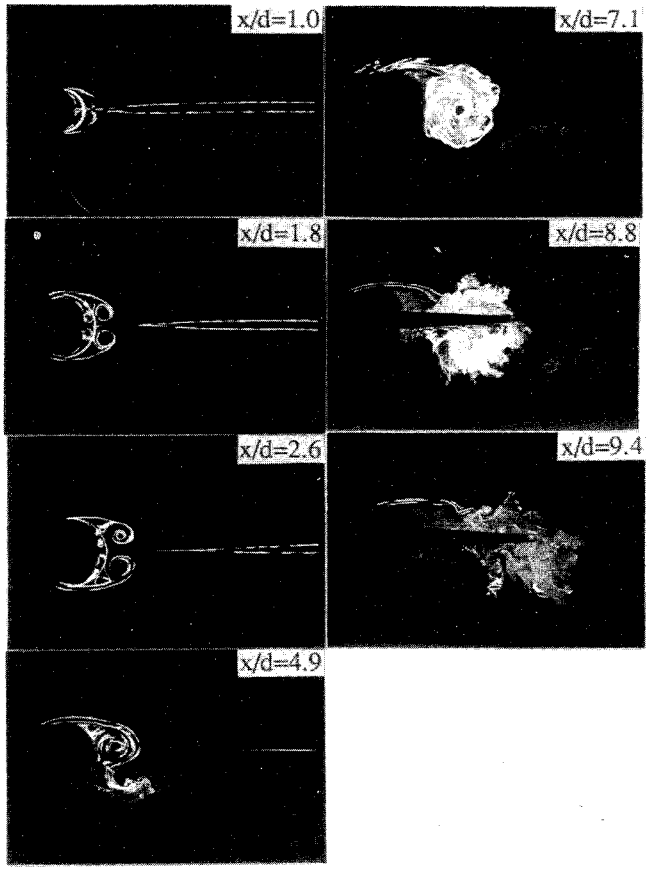

Fig. 2b Cross-sectional flow visualization showing flowfield development (α = 45 deg, ϕ = 0 deg, and $Re_d = 6 \times 10^3$).

As the vortices come in contact with the fin, they become less coherent, lift away from the body, and move away from the leeward ray; however, since the fin is positioned further downstream, the vortices are larger in size. The development of the vortex system with the fin at stations 2 [$(x/d)_f = 4.9$] and 1 [$(x/d)_f = 2.6$] is also shown in Ref. 6. Again, in both these cases the vortices remain symmetric, coherent, and attached to the body until they come in contact with the fin. At the fin, the vortices remain symmetric, but become less coherent and lift away from the body, and their centers are displaced away from the leeward ray by the presence of the fin. Because the fin is positioned closer to the nose, the vortices are smaller in size when they come in contact with the fin.

When the AOA is set at 45 deg, the vortex system is asymmetric, with the vortex on one side of the body separating from the body at a lower x/d location than the other vortex. The latter remains attached to the body and generally grows much larger than the first vortex, until it also separates from the body. This was shown previously for the same model with no fin attached by Acharya et al.[5] At this AOA, however, the axial location of the fin has a significant effect on the development of the flowfield. Figure 2b shows the development of the vortex system when the fin is placed at axial station 3 [$(x/d)_f = 7.1$]. The asymmetry in the flowfield with the fin at this axial location is clear. The vortices become asymmetric very close to the nose tip. At $x/d = 1.0$, the vortices are just beginning to form. At $x/d = 1.8$, the vortices are very coherent and the asymmetry is evident. The port vortex is clearly larger than the starboard vortex. This trend continues at $x/d = 2.6$. By $x/d = 4.9$, the port vortex is less coherent, distorted, and is beginning to lift away from the body. The starboard vortex continues to grow; it remains coherent and attached to the body. At $x/d = 7.1$, the leading edge of the fin, the port vortex is separated from the body and is much less coherent. The starboard vortex is much larger in size and still attached to the body, with its core located directly above the leeward ray of the model. At $x/d = 8.8$, the middle of the fin, the starboard vortex envelops the fin. It is even less coherent and slightly distorted, and its core is hard to locate. Also, it has separated from the body. The port vortex changes little and is located further away from the body. At the trailing edge of the fin, $x/d = 9.4$, the port vortex is faint and far away from the body. The starboard vortex has grown and is separated from the body, and it has been distorted further by the presence of the fin. At this AOA and fin location, the fin interacts with the starboard vortex to a much greater degree than with the port vortex. Because the latter is weak and far from the body at axial locations near the fin, its effect on the fin is minimal.

When the fin is positioned further from the nose, the flowfield is very similar to that at $(x/d)_f = 7.1$. However, when the fin is moved closer to the nose for an AOA of 45 deg, significant changes occur in the flowfield.[‡‡]

Figure 3 shows side and top views of the vortex-center trajectories for the four axial positions of the fin with $\alpha = 45$ deg,[§§] $\phi = 0$ deg, and $Re_d = 6 \times 10^3$. The vortex centers in this figure were obtained from the cross-sectional flow visualization photographs. The data end at the trailing edge of the fin because no flow visualization was performed beyond this point. The side views for $(x/d)_f = 7.1$ and 9.4 show that the port vortex separates from the body around $x/d = 4.9$. The starboard vortex remains attached to the body until about $x/d = 7.1$. Once a vortex separates, it moves quickly away from the body. When the fin is at station 4 [$(x/d)_f = 9.4$], the center of the starboard vortex passes the fin outboard of the fin tip, and the port vortex is out of the field of view. When the fin is at station 3 [$(x/d)_f = 7.1$], the center of the starboard vortex passes across the central portion of the fin, whereas the port vortex passes close to the leading edge of the fin tip but rapidly moves away further downstream. The trajectories for station 2 [$(x/d)_f = 4.9$] are slightly different. The starboard vortex remains closer to the body until just before the trailing edge of the fin. The port vortex is further away from the body at $x/d = 4.9$ than when the fin is at stations 3 and 4, but as it passes the fin, it does not move away from the body

[‡‡]These changes are described in detail in Section IV of the Addenda.

[§§]The symmetric vortex center trajectories for $\alpha = 30$ deg are described in Section V of the Addenda.

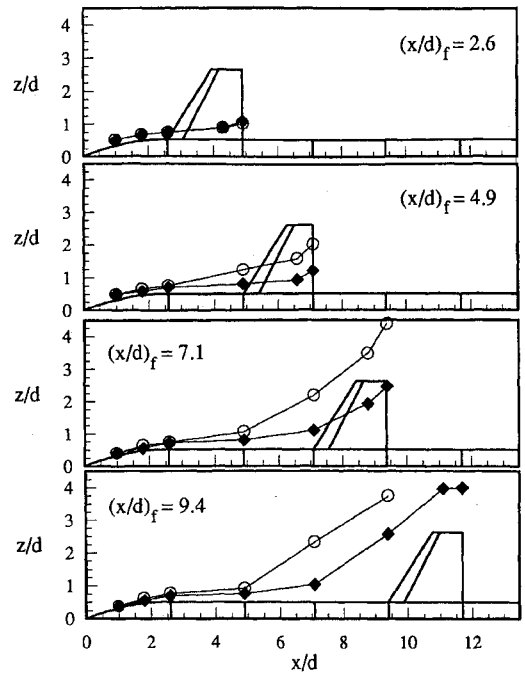

Side view

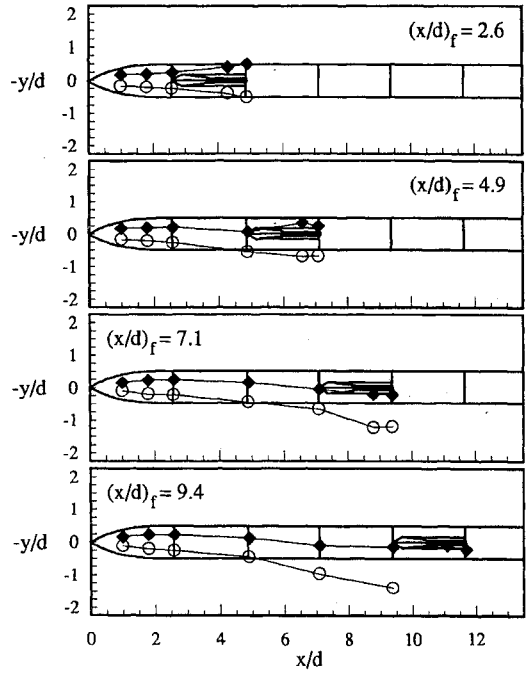

Top view

Fig. 3 Vortex center trajectories, side and top views (α = 45 deg, ϕ = 0 deg, and $Re_d = 6 \times 10^3$: ○, port vortex; ◇, starboard vortex.

as quickly. At this fin station, the centers of both vortices pass across the central portion of the fin. Finally, for station 1 [$(x/d)_f = 2.6$], the trajectories of the port and starboard vortices are nearly identical, indicating the flowfield has developed symmetrically with the fin at this axial location. Both vortices pass the fin close to the fin–body junction.

The top views for 45 deg also show that the vortex trajectories are symmetric at $(x/d)_f = 2.6$. At $(x/d)_f = 4.9$, the starboard vortex moves toward the leeward ray of the model ($y/d = 0$) as the port vortex begins to separate from the body. When it reaches the fin section, it moves away from the leeward ray and passes the fin to starboard. When the fin is at stations 3 [$(x/d)_f = 7.1$] and 4 [$(x/d)_f = 9.4$], the starboard vortex once again moves to the leeward ray as the port vortex separates; however, in these cases,

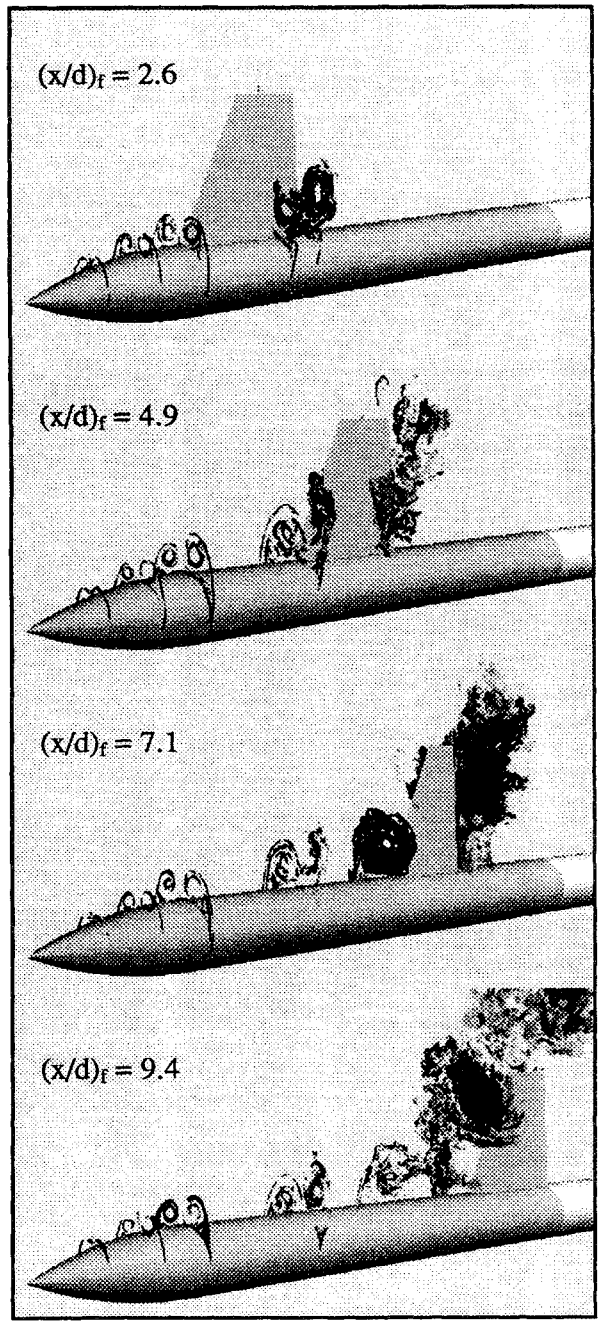

Fig. 4 Three-dimensional perspective views of flowfield (α = 45 deg, ϕ = 0 deg, and $Re_d = 6 \times 10^3$).

it remains there and appears to pass the fin on the port side. It was difficult to determine the exact center of the starboard vortex at the middle and trailing edge of the fin in cases where the vortex was greatly distorted because of contact with the fin. Nevertheless, it is clear that the axial location of the fin section has a significant effect on the development of the flowfield at an AOA of 45 deg.

The development of the flowfield in a three-dimensional perspective view is obtained by combining the cross-sectional flow visualizations with the vortex trajectories. This representation, shown in Fig. 4, helps further visualize the flowfield that exists under these conditions, especially the development of asymmetry in the vortex system at 45 deg[¶¶] and the changes in flowfield structure with changing axial fin location. No evidence of vortex bursting was found in any of the experiments, even for azimuthal positions of the fin away from the leeward ray. To ensure that flow unsteadiness was not a factor, multiple realizations of the flow

[¶¶]The three-dimensional views for α = 30 deg are described in Section VI of the Addenda.

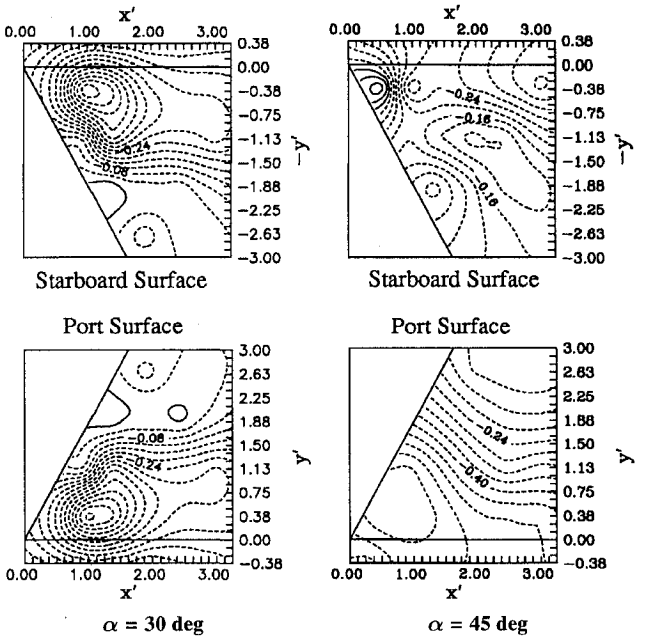

Fig. 5 Coefficient of pressure contours on the fin surfaces [$(x/d)_f = 7.1$, $\phi = 0$ deg, and $Re_d = 6 \times 10^3$].

visualizations and pressure measurements were obtained. The repeatability of observations and measurements was very good in all cases.

Pressure Variations on the Fin Surface

The pressure coefficient C_p contours on the port and starboard surfaces of the fin are shown in Fig. 5 for $(x/d)_f = 7.1$, $\phi = 0$ deg, and $Re_d = 6 \times 10^3$ at the two AOAs.*** Flow is from left to right. The fin is attached to the body at $y' = 0$, and its leading and trailing edges are at $x' = 0$ and 3.25, respectively. A projection of part of the missile body is also seen between $y' = 0$ and -0.38. Dashed lines indicate negative C_p values, whereas solid lines indicate positive C_p values. The pressure contours on the two sides of the fin are almost identical at 30 deg, confirming the symmetry of the flowfield. The most striking feature is the large low-pressure region near the fin–body junction. The concentration of pressure contours at half-span represents a rapid rise in pressure in the spanwise y' direction because of flow toward the fin surface. Near the tip of the fin, there is a region of higher pressure. This pressure distribution across the surface of the fin is a characteristic signature of a vortex near the surface. These pressure data can be compared directly with the $x/d = 8.8$ view in Fig. 2a, where the centers of the two vortices pass on either side of the fin slightly inboard of half-span. Further inboard of this location, near the fin–body junction, fluid is flowing away from the fin surface, creating a region of low pressure. Outboard of this location, near the tip, fluid is flowing toward the fin surface, creating a region of high pressure.

At an AOA of 45 deg, also shown in Fig. 5, the flow asymmetry results in a change in the vortex signature. The pressure distributions on the two sides of the fin are significantly different. On the starboard surface of the fin, the pressure is low near the fin–body junction because of separation of the flow from the body and a secondary recirculation. The pressure increases to a high-pressure region at half-span. The view at $x/d = 8.8$ in Fig. 2b shows inward flow toward the fin at this location. Further outboard of this location, the pressure decreases because of the presence of the starboard vortex. On the port surface of the fin, the pressure is low near the fin–body junction and steadily increases in the spanwise direction to a region of higher pressure at the fin tip, caused by fluid from the starboard vortex flowing around the tip of the fin. No significant effect of the weaker port vortex is seen.†††

***Section VII of the Addenda includes a discussion of the spanwise variations in these data.

†††Section VIII of the Addenda describes the effects of changing fin location.

Effects of Azimuthal Fin Position

When the fin is positioned along the leeward ray of the model at an AOA of 30 deg, the port and starboard vortices are located at equal distances from the port and starboard surfaces of the fin, respectively. Therefore, any effect of the vortex system on the two surfaces of the fin will be symmetric. As the azimuthal position of the fin changes, however, the position of the fin relative to the vortex system changes, and the effect of the vortex system on the two surfaces of the fin is no longer symmetric. However, since the overall flowfield is still symmetric, the effects of the vortex system at azimuthal positions of the fin to one side of the leeward ray ($+\phi$) are the same as those for azimuthal fin positions to the other side of the leeward ray ($-\phi$), if one compares the port surface pressure distribution at $+\phi$ to that on the starboard surface at $-\phi$ and vice versa.‡‡‡ These comparisons show that the vortex system remains symmetric as the azimuthal fin position is changed. Also, although the structures and trajectories of the vortices are affected at the fin locations, no upstream effects of azimuthal fin position on the flowfield were seen.

As the azimuthal position of the fin is changed in the asymmetric flowfield at 45 deg, the features and effects of the interaction between the vortex system and the fin at each axial location also change. At all axial fin locations, changing the azimuthal position of the fin changes the relative distance between each vortex and the fin surface. At axial locations near the fin section, the trajectories of the vortices are affected by the azimuthal position of the fin, especially at stations 1 and 2, which are close to the nose. However, the trajectory plots show little, if any, upstream effect of the azimuthal fin position on the paths of the vortices. Upstream effects of azimuthal fin position on the structures of the vortices are seen in cross-sectional flow-visualization photographs. In the first case, for fin station 1, the vortex on the side of the body to which the fin is placed is greatly affected at all x/d locations shown. The effect is not as pronounced for fin station 2 and is seen only immediately upstream of the fin's leading edge. The flow-visualization sequences at the last two fin stations show no upstream influence of the azimuthal fin position. The effects of the azimuthal position of the fin on the vortex structures and trajectories are examined in more detail in Kiedaisch.[6]

Effects of the Interaction at 30-deg AOA

The effects of the vortex system are best shown by an examination of the forces on the fin. When the fin is positioned on the leeward ray of the model for an AOA of 30 deg, the forces on each side of the fin have the same magnitude and are opposite in direction because of the symmetry of the flowfield. As the azimuthal position of the fin is changed, however, the forces on each side of the fin caused by the flow are no longer equal, and a net force and rolling moment are created. Calculations using potential-flow theory with no separation result in a total normal force coefficient C_{f_t} on the fin that exhibits a nearly sinusoidal variation with azimuthal fin position. The coefficient is zero when the fin is positioned along either the leeward ray or the windward ray of the model, reaches a maximum approximately 90 deg from the windward ray, and is at a minimum approximately 90 deg from the leeward ray.[1] Therefore, the magnitude of the total normal force on the fin at a given azimuthal position to one side of the leeward ray should be equal to the magnitude of the total normal force on the fin at the same azimuthal position on the other side of the leeward ray. However, these forces will act in opposite directions. For the coordinate system defined earlier, $C_{f_t} = 0$ at $\phi = 0$ and 180 deg. The maximum force in the positive direction should occur near $\phi = -90$ deg, and the maximum force in the negative direction should occur near $\phi = +90$ deg. Since the actual flowfield is separated and contains the vortex system, any differences between the forces obtained experimentally and the potential flow results may be attributed to the interaction of the fin with the vortex system.

Figure 6a shows the variation of C_{f_t} with ϕ for $\alpha = 30$ deg, $Re_d = 6 \times 10^3$, and fin station 3. This case shows all of the important features of the interaction and provides a base from which the effects of change in fin axial location can be seen. The variation in C_f and

‡‡‡Details are described in Section IX of the Addenda.

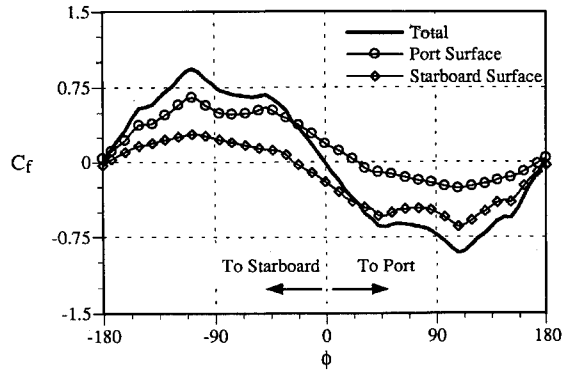

Fig. 6a Variation of normal force coefficient on fin with ϕ [α = 30 deg, $Re_d = 6 \times 10^3$, and $(x/d)_f = 7.1$].

the interaction with varying azimuthal fin position is similar at other axial fin stations; detailed results for these locations are described by Kiedaisch.[6]

Along with C_{ft}, the components for the port and starboard surfaces (C_{fp} and C_{fs}, respectively) are also shown in Fig. 6a. The outward normal to the port surface of the fin is the positive direction for the force coefficients. The forces are nearly perfectly antisymmetric about $\phi = 0$ deg, where $C_{ft} = 0$ as expected. At azimuthal angles starboard of the leeward ray (negative ϕ), the forces act on the fin in the positive direction. At azimuthal angles port of the leeward ray (positive ϕ), the forces act on the fin in the negative direction. Data for a rectangular-planform fin, presented by Mendenhall and Perkins,[1] show a small reversal in the direction of the force coefficient in the region $\phi = \pm 30$ deg that is not seen in the present data. The reasons for this difference are not clear; however, it may be caused by different experimental conditions and fin geometry. The fin used by Mendenhall and Perkins had a rectangular planform, a span equal to the body radius, and was placed 10.4 diameters from the missile nose. In the present experiment, a clipped-delta planform with a tapered leading edge was used. The span was four times the body radius, and the fin was not positioned further than 9.4 diameters from the missile nose. The fin used by Mendenhall and Perkins was smaller in size relative to the vortices, which may account for the different behavior of the force coefficients at azimuthal positions near the leeward ray. The C_{ft} curve shown in Fig. 6a is approximately sinusoidal as expected; however, three pairs of peaks are present. Each pair consists of a peak at some negative azimuthal angle and a corresponding peak at the complementary positive azimuthal angle. The two peaks in each pair correspond to forces that are identical in magnitude but opposite in direction. One pair of peaks is seen in each case at about $\phi = \pm 49$ deg. A second pair is seen at about $\phi = \pm 108$ deg, and a third, smaller pair of peaks occurs at about $\phi = \pm 151$ deg.

The pair of peaks at $\phi = \pm$ 108 deg represent the maximum positive and negative forces on the fin caused by the mean flow, not changes caused by the vortex system. Surface pressure contour plots substantiate this conclusion.[§§§] The most interesting pair of peaks occurs at about $\phi = \pm 49$ deg (Fig. 6a). These features are attributable to interaction between the fin and the vortex system. Between these peaks, over the range $\phi = -49$ deg to $+49$ deg, the total force on the fin is changed by the presence of the vortex system. At azimuthal angles beyond this range, the effects of the vortex system diminish. This conclusion is established by studying the flow visualizations and pressure-contour plots for azimuthal fin positions in this range.[¶¶¶] Plots of the spanwise pressure distributions on the leeward and windward sides of the fin show in more detail the influence of each vortex on the fin surface pressure.[****] Figure 6a shows a third pair of peaks in the C_{ft} curve at about $\phi = \pm 151$ deg. The C_{fp} and C_{fs} curves in the figure show that these peaks are caused by a change in the forces on the leeward side of the fin. Since these peaks occur at such high azimuthal angles, they are believed

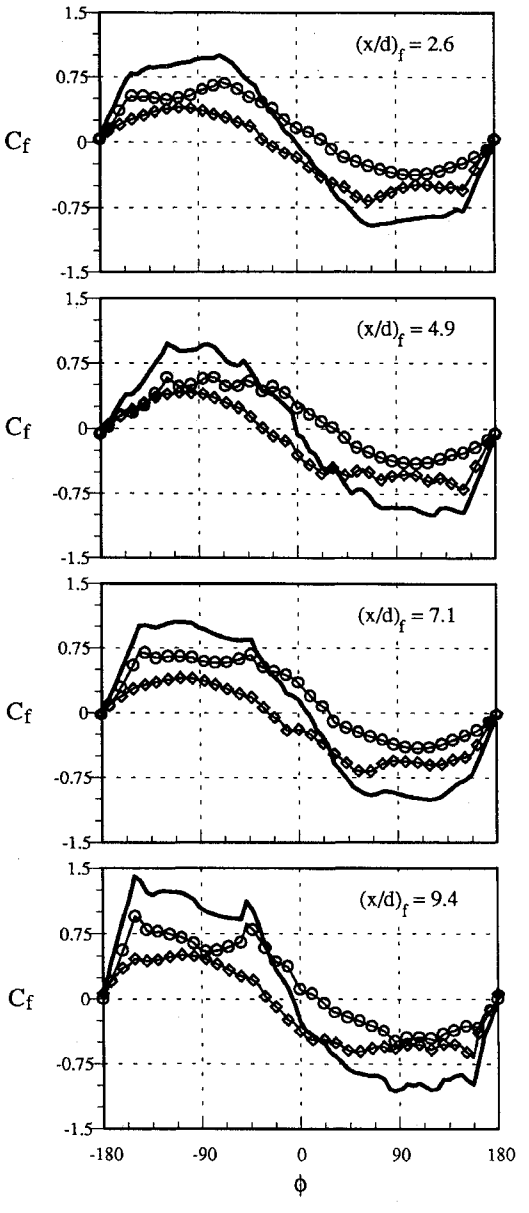

Fig. 6b Variation of normal force coefficient on fin with ϕ (α = 45 deg and $Re_d = 6 \times 10^3$): ——, total; ○, port surface; and ◇, starboard surface.

to be a feature of the external flow around the fin, which result when the separated, external flow on the leeward side of the fin reattaches as the leeward side of the fin changes to a windward orientation.[††††]

Effects of the Interaction at 45-deg AOA

At 45 deg, the flowfield and, hence, the interaction between the fin and the vortex system are significantly different at each of the four axial fin locations. Calculations similar to those reported by Mendenhall and Perkins could not be found in the literature for an asymmetric system of vortices. The flow visualization described earlier shows that at station 1, $(x/d)_f = 2.6$, the vortex system develops symmetrically because of the presence of the fin close to the nose. At station 2, $(x/d)_f = 4.9$, the flowfield develops asymmetrically; however, the fin is still relatively close to the nose, and thus the degree of asymmetry is small and both vortices remain close to the body throughout the interaction. At station 3, $(x/d)_f = 7.1$, a larger degree of asymmetry exists in the flowfield. The port vortex separates from the body ahead of the fin section, whereas the starboard vortex remains attached to the body until it reaches the fin and grows very large. The interaction is dominated by the starboard vortex, but the port vortex is still close enough to the fin to possibly

[§§§] See Section X of the Addenda for a detailed explanation.
[¶¶¶] See Section XI of the Addenda for a detailed explanation.
[****] See Section XII of the Addenda.

[††††] See Section XIII of the Addenda for a more detailed explanation.

have a small effect. Finally, at station 4, $(x/d)_f = 9.4$, the flowfield is dominated by the large, starboard vortex, which begins to separate from the body ahead of the fin section. The port vortex is very far from the body in this case and does not interact with the fin. The details of the interaction for selected ranges of azimuthal fin positions at each of these four axial fin locations are presented next.

Figure 6b shows the variations with azimuthal fin position in total normal force coefficient C_{f_t} for the fin, for each of the four axial fin locations at $Re_d = 6 \times 10^3$. The components for the port and starboard surfaces (C_{fp} and C_{fs}, respectively) are also shown. As expected, the force coefficient variations show large differences from the symmetric potential flow results. Also, distinct differences are apparent between the four axial fin locations. With the fin at station 1, the C_{f_t} variation with ϕ is almost perfectly antisymmetric about the leeward ray ($\phi = 0$ deg), as it was at all axial fin locations for $\alpha = 30$ deg. This confirms that the flowfield is symmetric as it makes contact with the fin at this axial location. The coefficient is zero when the fin is on the leeward and windward rays of the model, and the variation is somewhat sinusoidal in nature; however, two pairs of peaks are seen. One pair of large, broad peaks occurs at about $\phi = \pm 165$ deg, and a pair of smaller peaks occurs at about $\phi = \pm 162$ deg. The two peaks in each pair are identical in magnitude but opposite in direction. The variation of the total normal force coefficient C_{f_t} with azimuthal fin position for axial fin station 2 [$(x/d)_f = 4.9$] exhibits many irregularly spaced peaks over a large range of ϕ, but the overall variation is sinusoidal in nature. The coefficient C_{f_t} is no longer zero at $\phi = 0$ deg but is zero at $\phi = \pm 180$ deg.

To help explain this unusual behavior, it is necessary to examine in detail the cross-sectional flow visualizations and pressure coefficient contours at certain azimuthal fin positions in this range, as described later. When the fin is placed at station 3 [$(x/d)_f = 7.1$], there is a large degree of asymmetry in the flowfield, and the starboard vortex interacts with the fin to a much greater degree than does the port vortex. The vortex system has a smaller effect on the fin for azimuthal fin positions toward port than for fin positions toward starboard. This is clearly seen by studying the forces on the fin at different azimuthal positions in Fig. 6b. The forces on the fin are clearly asymmetric about the leeward ray, $\phi = 0$ deg, where the coefficient is nonzero. As the fin moves to starboard (negative ϕ), there is a sharp peak in the C_{f_t} curve at about $\phi = -43$ deg. This is the effect of the large, starboard vortex. As the fin moves toward port (positive ϕ), the C_{f_t} curve is relatively smooth. There is a broader dip in the curve around $\phi = +59$ deg, indicating that the vortex-induced forces are smaller, but that the effect of the vortices persists over a wider range of azimuthal angles to this side of the leeward ray. As for $\alpha = 30$ deg, Fig. 6b shows peaks in the C_{f_t} curve at azimuthal angles around $\phi = \pm 151$ deg.

As discussed earlier, these peaks are features of the external flow around the fin at these angles. In this case, the peak at $\phi = -151$ deg is much larger than that at $\phi = +151$ deg. This is caused by the asymmetry in the flowfield. The variation of the normal force coefficients with the fin at $(x/d)_f = 9.4$ is similar to that at the third fin station because the flowfield changes little at axial locations this far from the nose of the model. The C_{f_t} variation is clearly asymmetric about $\phi = 0$ deg, where there is a net force on the fin because of the asymmetry in the flowfield. There is a very large, sharp peak at about $\phi = -49$ deg, which represents the effect of the large, starboard vortex. At azimuthal angles to port of the leeward ray, there are some small bumps in the curve, but no distinct peaks are seen. This indicates that the vortex system has a reduced effect on the fin at these azimuthal positions. Once again, the C_{f_t} variation with azimuthal fin position for station 4 exhibits a smaller pair of peaks at $\phi = \pm 151$ deg, for the same reasons as discussed earlier.

To interpret these force coefficient variations and gain more information about the nature of the interaction, a detailed examination of the surface pressure contours and flow-visualization photographs was performed for each axial fin station.[‡‡‡‡]

Determining the Range of Interaction

A better understanding of the forces on the fin can be gained by studying the contributions to the normal forces of each side of the fin separately. Figure 6a shows that when the fin is positioned at negative azimuthal angles, peaks are present in the C_{fp} curve that correspond to the peaks in the C_{f_t} curve described earlier. However, the C_{f_s} curve is smooth and convex past a certain azimuthal angle. The opposite is true for positive azimuthal angles, where the C_{fp} curve is smooth and concave past a certain azimuthal angle and the C_{fs} curve exhibits the three peaks. Once the fin is positioned past a certain azimuthal angle, the windward side of the fin is not affected by the vortex system. The leeward side of the fin, however, is affected by the vortices over a wider range of azimuthal angles. Over a certain range of azimuthal angles to either side of $\phi = 0$ deg, the vortex system interacts with both sides of the fin. By examining the C_{fp} and C_{fs} curves in Fig. 6a,[§§§§] the range of azimuthal angles over which the vortex system interacts with each side of the fin can be defined. For this case, as the fin is moved toward port, it was determined that interaction with the port surface of the fin ends around $\phi = +32$ deg, whereas interaction with the starboard surface of the fin ends around $\phi = +54$ deg. As the fin is moved to starboard, a similar analysis of the pressure contour plots and Fig. 6a shows that interaction with the starboard surface ends around $\phi = -32$ deg and interaction with the port surface ends around $\phi = -54$ deg. Therefore, with the fin at station 3 for $\alpha = 30$ deg and $Re_d = 6 \times 10^3$, the port surface of the fin is influenced by the vortex system over the range -54 deg $< \phi < +32$ deg. The starboard surface of the fin is influenced by the vortex system over the range -32 deg $< \phi < +54$ deg. The changes in this range of interaction with fin axial location will be discussed later. The ranges of interaction are symmetric about the leeward ray for each case at this AOA. As the fin is placed axially further from the nose, the ranges increase because of the increase in size of the vortices as they travel downstream. These ranges are seen in the variations of the normal force coefficient components for each side of the fin as well. The C_{fp} and C_{fs} variations show that the force variations on the fin surface away from the vortex system are relatively smooth and sinusoidal, whereas the variations for the surface exposed to the vortex system show the deviations seen in the total force.

A similar analysis was used to determine the range of interaction for the 45-deg AOA. At axial fin station 1 (Fig. 6b), the port surface of the fin is influenced by the vortex system over the range -70 deg $< \phi < +32$ deg. The starboard surface of the fin interacts with the vortex system over the range -32 deg $< \phi < +70$ deg. The overall range is symmetric about $\phi = 0$ deg. At the second axial fin station, the range of interaction is much larger. The range for the port surface of the fin is -124 deg $< \phi < +32$ deg, and the range for the starboard surface is -32 deg $< \phi < +124$ deg. Even though the flowfield develops asymmetrically, the large effects of the azimuthal fin position on the structures and trajectories of the vortices cause a range of interaction that is symmetric about $\phi = 0$ deg for these flow conditions. For the third axial fin station, the starboard vortex dominates the wake, and distinct changes are seen in the forces on the port surface of the fin over a small range of negative azimuthal angles. At positive azimuthal angles, changes seen on the starboard surface of the fin are less distinct but occur over a wider range. The port surface of the fin is influenced by the vortex system over the range -43 deg $< \phi < +27$ deg. The starboard surface of the fin is influenced by the vortex system over the range -32 deg $< \phi < +54$ deg. The range of interaction for the fourth axial fin station is very similar to that at the third station. It is slightly larger, however, because of the growth of the starboard vortex. The port surface of the fin interacts with the vortex system over the range -49 deg $< \phi < +16$ deg, and the starboard surface of the fin interacts over the range -32 deg $< \phi < +54$ deg. More details may be found in Kiedaisch.[6]

Effects of Change in Fin Axial Location

The differences in the interaction between the vortex system and the fin that occur as the axial location of the fin is changed were

[‡‡‡‡]See Section XIV of the Addenda.

[§§§§]See also Fig. 10 in the Addenda.

studied in detail.[¶¶¶] For $\alpha = 30$ deg, and $Re_d = 6 \times 10^3$, the overall range of azimuthal angles over which interaction occurred between the fin and the vortex system remained constant up to $(x/d)_f = 7$ and increased slightly beyond this value. The range in which both sides of the fin interact with the vortex system increased with increasing $(x/d)_f$. This was because of the growth of the vortices with increasing x/d. Similar trends were seen at higher Reynolds numbers. At $\alpha = 45$ deg, the interaction was more complex.

Conclusions

A detailed examination of the interaction of a generic fin with both a symmetric and an asymmetric pair of vortices in the leeside wake of a missile model has provided information on the effect of the interaction on the fin, as well as information on the effect of the fin position on the vortex system. A flow visualization study was performed, and the formation and growth of the nose-tip vortices, the trajectories of these vortices, and the structures of these vortices at the fin section during the interaction were documented.

At $\alpha = 30$ deg, the vortices developed symmetrically and remained symmetric throughout the interaction with the fin at all four axial fin locations. At the fin section, the structures and trajectories of the vortices were affected at different azimuthal fin positions. No upstream influence of the axial or azimuthal fin positions was seen. However, although the axial position of the fin did not affect the upstream development of the vortices, it did affect the location at which the vortices separate from the body. In contrast, at $\alpha = 45$ deg, the flowfield was significantly different for each axial fin location. At the first axial fin location, the vortices developed symmetrically, whereas at the other three axial fin locations, the vortices developed asymmetrically, showing an influence of the axial fin location on the flowfield. At the two axial fin locations closest to the nose, an upstream influence of the azimuthal fin position on the structures of the vortices was observed. No vortex breakdown was observed in the present experiments.

The flow visualization, coupled with pressure and force data, enabled a greater understanding of the vortex-induced effects on the loading of the fin, the range of interaction, and the effects of axial fin position. Although the Reynolds number range encountered in practice is much higher, several features of the flow and the vortex–fin interactions should carry over, making the present results valuable. Experiments with slender bodies at higher Reynolds numbers have very similar behavior of the flowfield, including the development of an asymmetric vortex system.[4] In addition, the data are detailed enough to be very valuable in the validation and verification of different computational modeling techniques. The results of this study can be useful in missile design. Knowledge of the nature of the flowfield around the fin at different axial and azimuthal positions can be used to determine optimal fin placement on the missile. The effectiveness of the fin as a control surface can be estimated from the force data presented for different axial and azimuthal fin positions. These results can be extended to multifin configurations if the fins are placed so that they do not alter the upstream development of the flowfield and if the assumption is made that the presence of additional fins does not change the characteristics of the interaction, as described in this paper for a single fin.

Acknowledgments

This research was carried out with the help of a grant from the U.S. Army Research Office, DAAL03-91-G-0043, monitored by Thomas Doligalski.

References

[1]Mendenhall, M. R., and Perkins, S. C., Jr., "Vortex Induced Characteristics of Missiles in Unsteady Maneuvers," AIAA Paper 89-0344, Jan. 1989.

[2]Washburn, A. E., Jenkins, L. N., and Ferman, M. A., "Experimental Investigation of Vortex-Fin Interaction," AIAA Paper 93-0050, Jan. 1993.

[3]Bodstein, G. C. R., George, A. R., and Hui, C. Y., "Vortex/Surface Interaction," AIAA Paper 93-0863, Jan. 1993.

[4]Ericsson, L. E., and Reding, J. P., "Asymmetric Vortex Shedding from Bodies of Revolution," *Tactical Missile Aerodynamics*, edited by M. J. Hemsch and J. N. Nielsen, Vol. 104, Progress in Astronautics and Aeronautics, AIAA, New York, 1986, pp. 243–296.

[5]Acharya, M., Kiedaisch, J., and Mohammad Hassan, M., "Asymmetric Vortical Flows Over Slender Bodies with Appendages," IIT Fluid Dynamics Research Center, TR, Chicago, IL, June 1994.

[6]Kiedaisch, J. W., "Experimental Investigation of the Interaction of Missile Tip Vortices with a Control Surface," M.S. Thesis, Mechanical and Aerospace Engineering Dept., Illinois Inst. of Technology, Chicago, IL, 1994.

[¶¶¶]See Section XV of the Addenda for results.